Case Studies in Thermal Engineering 13 (2019) 100413

Contents lists available at ScienceDirect

Case Studies in Thermal Engineering

journal homepage: www.elsevier.com/locate/csite

Numerical study of MHD effective Prandtl number boundary layer flow of γ Al_2O_3 nanofluids past a melting surface

N. Vishnu Ganesh[a], Qasem M. Al-Mdallal[b,*], P.K. Kameswaran[c]

[a] Department of Mathematics, Ramakrishna Mission Vivekananda College, Mylapore, Chennai, 600004, Tamil Nadu, India
[b] Department of Mathematical Sciences, United Arab Emirates University, P.O. Box 15551, Al Ain, Abu Dhabi, United Arab Emirates
[c] Department of Mathematics, VIT University, Vellore, Tamil Nadu, India

ARTICLE INFO

Keywords:
Effective Prandtl number
Melting heat transfer
MHD
Nanofluids
Non-linear thermal radiation

ABSTRACT

This research article numerically studies the influences of an effective Prandtl number along with magnetic field on the melting heat transport characteristics of Ethylene glycol/Water with gamma Al_2O_3 nanoparticles over a stretching sheet. To analyse the impacts of effective Prandtl number, the non-dimensional melting heat transfer boundary conditions are derived for the first time with and without effective Prandtl number. A non-linear form of thermal radiation is used. The experimental based thermo-physical properties of gamma Al_2O_3 nanofluids are considered. The electric conductivities of Al_2O_3, water and ethylene glycol are used to calculate of effective electric conductivity to study the magnetic field effects. Mathematical models are developed and solved by numerical technique based on the Iterative Power Series (IPS) method with shooting strategy. The numerical outcomes are discussed through plots and tables.

1. Introduction

The exploration on the topic of nanofluid heat transfer characteristics together with melting heat transport past a stretchable surface has been considered by the recent researchers because of its applications in many engineering and industrial processes. The Nanofluid concept was first proposed by Choi [1]. In recent decade, Nanofluids are used in industries to improve the thermal performance of the thermal systems [2–21]. Different aspects on the boundary layer flow of nanofluids together with melting heat transfer have been studied through similarity analysis [22–25]. In the above-mentioned similarity analysis, the governing PDE's along with the boundary conditions have been converted to non-dimensional ODE's using appropriate transformations. The non-dimensional form of melting heat transfer boundary condition depends on two parameters namely Prandtl number and Melting heat parameter. In recent years, fractional model fluid flow problems are also studied by the following researchers [26,27].

The studies on the flow phenomena of γ Al_2O_3 nanofluids show its importance in cooling processes [28–37]. Moghaieb et al. [38] used γ $Al_2O_3-H_2O$ nanofluid to cool an engine. The studies of Vishnu Ganesh et al. [39] and Rashidi et al. [40] reported that the flow characteristics of γ Al_2O_3 nanofluids over stretchable surface through similarity solutions. They used experimental based thermo physical properties in their studies. Rashidi et al. [40] considered an effective Pr on the flow of γ Al_2O_3 nanofluid and obtained some significant results on the temperature of γ Al_2O_3 nanofluids. Vishnu Ganesh et al. [41] investigated the non-linear thermal radiation effects on Marangoni boundary layer of γ Al_2O_3 nanofluids with effective *Pr*. Currently, Vishnu Ganesh et al. [42] analysed the magnetic field effects on the Marangoni boundary layer of γ Al_2O_3 nanofluids in the presence of effective *Pr*.

This work is devoted to derive the melting heat boundary condition for γ Al_2O_3 nanofluids with an effective *Pr* model. The

* Corresponding author.
E-mail address: q.almdallal@uaeu.ac.ae (Q.M. Al-Mdallal).

https://doi.org/10.1016/j.csite.2019.100413
Received 7 January 2019; Received in revised form 3 February 2019; Accepted 9 February 2019
Available online 12 February 2019
2214-157X/

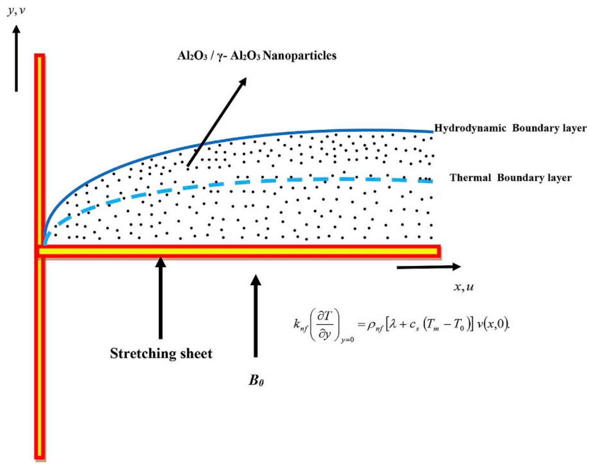

Fig. 1. Physical model and coordinate system.

numerical results are discussed for γ Al_2O_3 nanofluids over a stretching sheet.

2. Formulation of the problem

Consider a 2D incompressible, laminar and steady state boundary layer flow of water/ethylene glycol based γ Al_2O_3 nanofluids towards a horizontal stretching sheet under the influence of thermal radiation. The physical model of the flow is shown in Fig. 1. The following assumptions are considered to develop the mathematical model:

(i) It is assumed that the sheet is stretching in the velocity $u_w(x) = ax$, where a is a constant.
(ii) The applied transverse magnetic field strength is B_0 in which the electric field and magnetic Reynolds number are negligible.
(iii) The temperature in the free-stream condition (T_∞) is greater than the temperature of the melting sheet (T_m).
(iv) A thermal equilibrium state has been assumed between the base fluids and nanoparticles. Considering the above assumptions, the governing equations with thermo-physical properties of nanofluids (Table 1.) can be written as

$$\frac{\partial u}{\partial x} = -\frac{\partial v}{\partial y} \tag{1}$$

$$v\frac{\partial u}{\partial y} + u\frac{\partial u}{\partial x} + \frac{\sigma_{nf}\, B_0^2\, u}{\rho_{nf}} = \frac{\mu_{nf}}{\rho_{nf}}\frac{\partial^2 u}{\partial y^2}, \tag{2}$$

$$v\frac{\partial T}{\partial y} + u\frac{\partial T}{\partial x} + \frac{1}{(\rho C_p)_{nf}}\left(\frac{\partial q_r}{\partial y}\right) = \frac{k_{nf}}{(\rho C_p)_{nf}}\frac{\partial^2 T}{\partial y^2}. \tag{3}$$

The no-slip boundary conditions for flow over stretching sheet with melting heat transfer are

$$u = u_w,\ \ v = 0,\ T = T_m \text{ at } y = 0,$$
$$u \to 0,\ T \to T_\infty \text{ as } y \to \infty, \tag{4}$$

and

$$k_{nf}\left(\frac{\partial T}{\partial y}\right)_{y=0} = \rho_{nf}\left[\lambda + c_s\,(T_m - T_0)\right]\ v(x, 0), \tag{4.1}$$

Where u and v are the velocity components along the axis x and y, respectively, q_r is the radiative heat flux, λ is the latent heat of the fluid and c_s is the heat capacity of the solid surface. Equation (4.1) shows the relation between the heat conducted to the melting

Table 1
Thermo physical properties of water, ethylene glycol and alumina.

	ρ (kg/m^3)	C_p (J/kg K)	k (W/m K)	σ (Ω. m)$^{-1}$	*Pr*
Pure water (H_2O)	998.3	4182	0.60	0.05	6.96
Ethylene glycol ($C_2H_6O_2$)	1116.6	2382	0.249	1.07×10^{-7}	204
Alumina (Al_2O_3)	3970	765	40	10^{-12}	–

surface, the sensible heat mandatory to enhance the temperature of the solid T_0 and the melting temperature T_m of the solid surface.

The radiative heat flux in non-linear form (Rosseland approximation) is given by Refs. [43,44].

$$q_r = -\frac{4\,\sigma^*}{3\,k^*}\frac{\partial T^4}{\partial y} = -\frac{16\,\sigma^*}{3\,k^*}T^3\frac{\partial T}{\partial y} \tag{5}$$

where k^* is the Stefan- Boltzman constant and also σ^* is the mean absorption coefficient.

Now Eq. (3) can be expressed as

$$v\frac{\partial T}{\partial y} + u\frac{\partial T}{\partial x} - \frac{\partial}{\partial\, y}\left[\left(\frac{k_{nf}}{(\rho C_p)_{nf}} + \frac{16\,\sigma^* T^3}{3\,(\rho C_p)_{nf} k^*}\right)\frac{\partial T}{\partial y}\right] = 0. \tag{6}$$

The relationships between the effective dynamic density (ρ_{nf}), the heat capacitance $\left((\rho C_p)_{nf}\right)$, the effective electric conductivity $\left(\frac{\sigma_{nf}}{\sigma_f}\right)$, dynamic viscosity $\left(\frac{\mu_{nf}}{\mu_f}\right)$, effective thermal conductivity $\left(\frac{k_{nf}}{k_f}\right)$ and effective Pr $\left(\frac{\mathrm{Pr}_{nf}}{\mathrm{Pr}_f}\right)$ are given as follow [28–31]:

$$\rho_{nf} - (1-\varphi)\rho_f - \varphi\rho_s = 0,\ (\rho C_p)_{nf} - (1-\varphi)(\rho C_p)_f - \varphi(\rho C_p)_s = 0,\ \frac{\sigma_{nf}}{\sigma_f} = \left[1 + \frac{3\left(\frac{\sigma_s}{\sigma_f} - 1\right)\varphi}{\left(\frac{\sigma_s}{\sigma_f} + 2\right) - \left(\frac{\sigma_s}{\sigma_f} - 1\right)\varphi}\right], \tag{7}$$

$$\frac{\mu_{nf}}{\mu_f} = 123\,\varphi^2 + 7.3\ \varphi + 1,\ (\text{for}\ \gamma\ \mathrm{Al_2O_3} -\ \text{Water}), \tag{8}$$

$$\frac{\mu_{nf}}{\mu_f} = 306\,\varphi^2 - 0.19\ \varphi + 1,\ (\text{for}\ \gamma\ \mathrm{Al_2O_3} -\ \text{Ethylene glycol}), \tag{9}$$

$$\frac{k_{nf}}{k_f} = 4.97\,\varphi^2 + 2.72\ \varphi + 1,\ (\text{for}\ \gamma\ \mathrm{Al_2O_3} -\ \text{Water}) \tag{10}$$

$$\frac{k_{nf}}{k_f} = 28.905\,\varphi^2 + 2.8273\ \varphi + 1\ ,\ (\text{for}\ \gamma\ \mathrm{Al_2O_3} -\ \text{Ethylene glycol}), \tag{11}$$

$$\frac{\mathrm{Pr}_{nf}}{\mathrm{Pr}_f} = 82.1\,\varphi^2 + 3.9\ \varphi + 1,\ (\text{for}\ \gamma\ \mathrm{Al_2O_3} - \text{Water}), \tag{12}$$

$$\frac{Pr_{nf}}{Pr_f} = 254.\ 3\,\varphi^2 - 3\ \varphi + 1,\ (\text{for}\gamma\ \mathrm{Al_2O_3} -\ \text{Ethylene glycol}), \tag{13}$$

where φ is the solid volume fraction of nanofluid.

By applying the similarity transformations.

$$\frac{\eta}{y} = \sqrt{\frac{a}{\nu_f}},\ \frac{u}{f\,'(\eta)} = ax\ ,\ \frac{v}{f\,(\eta)} = -(a\ \nu_f)^{1/2}\ \text{and}\ \theta = \frac{T - T_\infty}{T_\infty - T_m}, \tag{14}$$

the governing boundary layer equations (2) and (6) take the following non-dimensional form

$$f\,''' + \frac{1}{(123\,\varphi^2 + 7.3\ \varphi + 1)}\left[\left(1 - \varphi + \varphi\left(\frac{\rho_s}{\rho_f}\right)\right)(f\,f\,'' - f\,'^{\,2}) - \left[1 + \frac{3\left(\frac{\sigma_s}{\sigma_f} - 1\right)\varphi}{\left(\frac{\sigma_s}{\sigma_f} + 2\right) - \left(\frac{\sigma_s}{\sigma_f} - 1\right)\varphi}\right]Mn\,f\,'\right]$$
$$= 0\ ,\ (\text{for ? Al2O3} - \text{Water}), \tag{15}$$

$$f\,''' + \frac{1}{(306\,\varphi^2 - 0.19\ \varphi + 1)}\left[\left(1 - \varphi + \varphi\left(\frac{\rho_s}{\rho_f}\right)\right)(f\,f\,'' - f\,'^{\,2}) - \left[1 + \frac{3\left(\frac{\sigma_s}{\sigma_f} - 1\right)\varphi}{\left(\frac{\sigma_s}{\sigma_f} + 2\right) - \left(\frac{\sigma_s}{\sigma_f} - 1\right)\varphi}\right]Mn\,f\,'\right]$$
$$= 0\ ,\ (\text{for ? Al2O3} -\ \text{Ethylene glycol}), \tag{16}$$

$$\theta\,''\,[1 +\ R_d\,A(\theta(1 - \theta_w) + \theta_w)^3] + R_d\,A[3\,\theta\,'^2(1 - \theta_w)(\theta(1 - \theta_w) + \theta_w)^2] + B(f\ \theta\,') = 0, \tag{17}$$

where

$$A = (4.97\,\varphi^2 + 2.72\ \varphi + 1)^{-1},\ (\text{for}\gamma\ \mathrm{Al_2O_3} -\ \text{Water}),$$

$$A = (28.905\,\varphi^2 + 2.8273\ \varphi + 1)^{-1},\ (\text{for}\gamma\ \mathrm{Al_2O_3} -\ \text{Ethylene glycol}),$$

$$B = \frac{\Pr_f\left(1 - \varphi + \varphi\left(\frac{\rho_s}{\rho_f}\right)\right)(82.1\ \varphi^2 + 3.9\ \varphi + 1)}{123\ \varphi^2 + 7.3\ \varphi + 1} \text{(with effective Pr for } \gamma \text{ Al}_2\text{O}_3 - \text{Water),}$$

$$B = \frac{\Pr_f\left(1 - \varphi + \varphi\left(\frac{\rho_s}{\rho_f}\right)\right)(254.3\ \varphi^2 - 3\ \varphi + 1)}{306\ \varphi^2 - 0.19\ \varphi + 1} \text{(with effective Pr for } \gamma \text{ Al}_2\text{O}_3 - \text{ Ethylene glycol),}$$

$$B = \frac{\Pr_f\left(1 - \varphi + \varphi\left(\frac{(\rho C_p)_s}{(\rho C_p)_f}\right)\right)}{4.97\ \varphi^2 + 2.72\ \varphi + 1} \text{(without effective Pr for} \gamma \text{ Al}_2\text{O}_3 - \text{Water),}$$

$$B = \frac{\Pr_f\left(1 - \varphi + \varphi\left(\frac{(\rho C_p)_s}{(\rho C_p)_f}\right)\right)}{28.905\ \varphi^2 + 2.8273\ \varphi + 1}, \text{ (without effective Pr for } \gamma \text{ Al}_2\text{O}_3 - \text{ Ethylene glycol).}$$

The transformed boundary conditions are

$$f\,'(0) - 1 = 0,\ f\,'(\infty) = 0,\ \theta(0) = 0,\ \theta(\infty) - 1 = 0, \tag{18}$$

$$\frac{\Pr_f\left(1 - \varphi + \varphi\left(\frac{\rho_s}{\rho_f}\right)\right)(82.1\ \varphi^2 + 3.9\ \varphi + 1)}{123\ \varphi^2 + 7.3\ \varphi + 1} f(0) + \left((1 - \varphi) + \varphi\left(\frac{(c_p)_s}{(c_p)_f}\right)\right) M\ \theta\,'(0) = 0\,,$$

(with effective *Pr* for γ *Al_2O_3-Water*),

$$\frac{\Pr_f\left(1 - \varphi + \varphi\left(\frac{\rho_s}{\rho_f}\right)\right)(254.3\ \varphi^2 - 3\ \varphi + 1)}{306\ \varphi^2 - 0.19\ \varphi + 1} f(0) + \left((1 - \varphi) + \varphi\left(\frac{(c_p)_s}{(c_p)_f}\right)\right) M\ \theta\,'(0) = 0\,,$$

(with effective *Pr* for γ *Al_2O_3- Ethylene glycol*),

$$Pr_f\left(1 - \varphi + \varphi\left(\frac{\rho_s}{\rho_f}\right)\right) f(0) + M\ (4.97\ \varphi^2 + 2.72\ \varphi + 1)\,\theta\,'(0) = 0\ \text{, (without effective Pr for } \gamma \text{ Al}_2\text{O}_3 - \text{Water),}$$

$$Pr_f\left(1 - \varphi + \varphi\left(\frac{\rho_s}{\rho_f}\right)\right) f(0) + M\ (28.905\ \varphi^2 + 2.8273\ \varphi + 1)\,\theta\,'(0) = 0, \text{ (without effective Pr for } \gamma \text{ Al}_2\text{O}_3 - \text{ Ethylene glycol),} \tag{18.1}$$

where $Mn = \frac{\sigma_f B_0^2}{\rho_f\ a}$ is the magnetic parameter, $R_d = \frac{16\ \sigma^* T_\infty^3}{3\ k^* k_f}$ is the radiation parameter, $\theta_w = \frac{T_m}{T_\infty}$ is the temperature ratio parameter, $M = \frac{(c_p)_f\ [T_\infty - T_m]}{\lambda + c_s\ [T_m - T_0]}$ is the melting parameter which is the combination of the Stefan numbers for the solid and liquid phases, and $\Pr_f = \frac{\nu_f}{\alpha_f}$ is the Prandtl number.

The skin friction coefficient C_f, is given by

$$C_f = \frac{-2\,\mu_{nf}}{\rho_f\ u_w^2}\left(\frac{\partial u}{\partial y}\right)_{y=0}.$$

Using Eqn. (14), the skin friction can be derived as

$$\frac{1}{2}\,\text{Re}_x^{1/2} C_f = -(123\ \varphi^2 + 7.3\ \varphi + 1)\ f\,''(0), \text{(for } \gamma \text{ Al}_2\text{O}_3 - \text{Water),}$$

$$\frac{1}{2}\,\text{Re}_x^{1/2} C_f = -(306\ \varphi^2 - 0.19\ \varphi + 1)\ f\,''(0), \text{(for } \gamma \text{ Al}_2\text{O}_3 - \text{ Ethylene glycol),} \tag{19}$$

where $\text{Re}_x = \frac{x\ u_w(x)}{\nu_f}$ the local Reynolds number and $\text{Re}_x^{1/2} C_f$ is the local skin friction coefficient.

The Nusselt number (Nu_x) is defined as

$$Nu_x = \frac{x\ q_w}{k_f\,(T_w - T_\infty)},$$

where $q_w = -k_{nf}\left(\frac{\partial T}{\partial y}\right)_{y=0} + (q_r)_w$ represents the local surface heat flux.

Using the similarity transformations (14), we derived the following Nusselt number

Table 2
Comparison of results for -θ′(0).

Pr	Hamad (2011)	Present results ($\phi = 0, Mn = 0, Rd = 0$ and $M = 0$)
0.2	1.16909	0.16908858
2	0.91136	0.91135764
7	1.89540	1.89540311
20	3.3539	3.35390647

$$\mathrm{Re}_x^{-1/2}Nu_x = -(4.97\,\varphi^2 + 2.72\,\varphi + 1)\,\theta\,'(0)\left[1 + \frac{R_d\,(\theta_w)^3}{(4.97\,\varphi^2 + 2.72\,\varphi + 1)}\right], \text{(for } \gamma\ \mathrm{Al_2O_3}\text{—Water)},$$
$$\mathrm{Re}_x^{-1/2}Nu_x = -(28.905\,\varphi^2 + 2.8273\,\varphi + 1)\,\theta\,'(0)\left[1 + \frac{R_d\,(\theta_w)^3}{(28.905\,\varphi^2 + 2.8273\,\varphi + 1)}\right], \text{(for } \gamma\ \mathrm{Al_2O_3}\text{— Ethylene glycol)}. \tag{20}$$

3. Numerical method for the solutions

The transformed governing boundary layer equations in (15)–(17) with the corresponding no-slip and melting heat boundary conditions in (18) and (18.1) are solved using the Iterative Power Series (IPS) Method along with a shooting technique [45,46]. The BVP is initially converted into an IVP and then the IVP is solved numerically by taking the step size of $\Delta\eta = 0.01$ with $\eta_\infty = 20$, where η_∞ represents the infinity in the η domain. The solutions are obtained with the convergence criterion of 10^{-8} in all cases.

4. Results and discussion

Before solving the present problem using above numerical scheme, a code validation has been made with Hamad [2] for the clear fluid case. The results obtained for $-\theta\,'(0)$ are in good agreement which is tabulated in Table 2. In order to know the significance of the effective *Pr* on the melting heat boundary condition, the above numerical procedure is applied to find the numerical solutions of transformed governing boundary layer equations with the corresponding no-slip and melting heat boundary conditions. The numerical results are plotted to understand the importance of physical parameters on the velocity and temperature profiles, skin friction coefficient and reduced Nusselt number for both the cases with effective *Pr* and without effective *Pr*. The nanofluids considered in the study are γ Al_2O_3-*Water* and γ Al_2O_3- *Ethylene glycol* and the Prandtl numbers are fixed as 6.96 and 204 for the base fluids water and ethylene glycol respectively. In all graphical illustrations, the solid lines are used to represent the with effective *Pr* case and the dashed lines are used to represent the without effective *Pr* case.

The effects of ϕ and *Mn* on the velocity profile of the nanofluids γ Al_2O_3 - *Water* and γ Al_2O_3 - *Ethylene glycol* are depicted in Fig. 2(a)and (b) respectively. It can be seen that an increment in ϕ accelerates the velocity profile and the increasing values of *Mn* decelerate the velocity profile of the nanofluids in both the cases with and without effective *Pr*. On comparing theses figures, a greater velocity profile is observed for γ Al_2O_3- *Ethylene glycol*. The presence of effective *Pr* leads to increase the nanomomentum boundary layer thickness.

It is worth mentioning that our intensive simulations show that M, Mn and R_d have similar effect on the temperature profile of nanofluids, θ. Therefore, we will discuss only the effect of *Mn*. Fig. 3(a)and (b) show the effect of *Mn* on the temperature profile of γ Al_2O_3-*Water* and γ Al_2O_3- *Ethylene glycol* nanofluids respectively with melting heat transfer. It is clear that an increment in the *Mn* increases the nanothermal boundary layer thickness. This is because, the increasing values of *Mn* leads to increase B_0. Due to the increase of B_0, a force called Lorentz force is generated in the flow region which leads to increase the thermal boundary layer thickness. The temperature of γ Al_2O_3-*Water* is higher than γ Al_2O_3- *Ethylene glycol*. It is also noted that the effective Prandtl number has a significant effect on the temperature profile. The inclusion of effective *Pr* increases the nanothermal boundary layer thickness of γ Al_2O_3- *Ethylene glycol* nanofluid and decreases the nanoboundary layer thickness of γ Al_2O_3- Water nanofluid.

The effect of ϕ on the temperature profile is shown in Fig. 4(a)and (b). It is observed that the increasing values of nanoparticle volume fraction parameter (ϕ) increase the temperature profile and decreases the nanothermal boundary layer thickness for γ Al_2O_3-*Water* nanofluid (Fig. 4(a)). The nanoparticle volume fraction parameter shows a notable result on the temperature of γ Al_2O_3-*Ethylene glycol* nanofluid. The increasing values of ϕ enhance the temperature profile in the presence of effective *Pr* and diminish the temperature profile in the absence of effective *Pr*. On observing theses figures, it is noted that the nanothermal boundary layer thickness of γ Al_2O_3-*Water* decreases in the absence of effective *Pr* and the nanothermal boundary layer thickness of γ Al_2O_3- *Ethylene glycol* increases in the absence of effective *Pr*.

The variation of skin friction coefficient with *Mn* and ϕ for γ Al_2O_3-*Water* and γ Al_2O_3- *Ethylene glycol* nanofluids in both cases with and without effective *Pr* is shown in Fig. 5(a)and (b). The magnitude of skin friction coefficient increases with *Mn* and ϕ. It increases for γ Al_2O_3- *Ethylene glycol* and decreases for γ Al_2O_3- *Water* in the presence of effective *Pr*.

Fig. 6 (a) & 6(b) display the variation of reduced Nusselt number of γ Al_2O_3-*Water* and γ Al_2O_3- *Ethylene glycol* nanofluids with magnetic parameter and melting heat parameter. The magnetic parameter is taken as x- axis and the reduced Nusselt number is taken as y- axis. It is observed that the magnitude of reduced Nusselt number increases with *Mn* and *M* for both γ Al_2O_3 - *Water* and γ Al_2O_3 - *Ethylene glycol* nanofluids. The magnitude of reduced Nusselt number is higher for γ Al_2O_3 - *Ethylene glycol* and also it is higher in the presence of effective *Pr*.

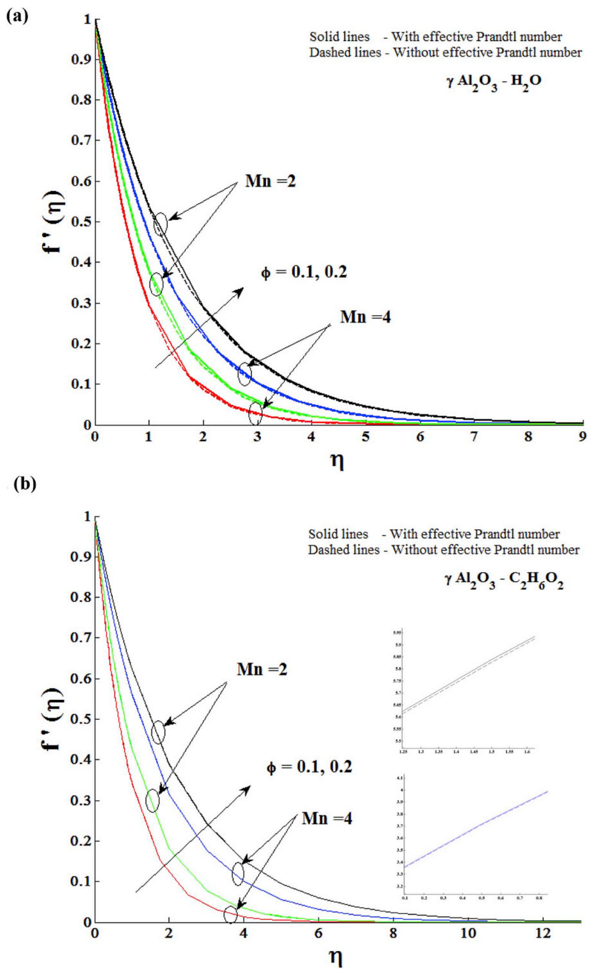

Fig. 2. Effects of nanoparticle volume fraction (ϕ) and magneitc parameter (Mn) on velocity profile with Rd = 2.5, $\theta_w = 1.5$ and M = 2 (a) γ $Al_2O_3 - H_2O$ with $Pr = 6.96$ (b) γ $Al_2O_3 - C_2H_6O_2$ with $Pr = 204$.

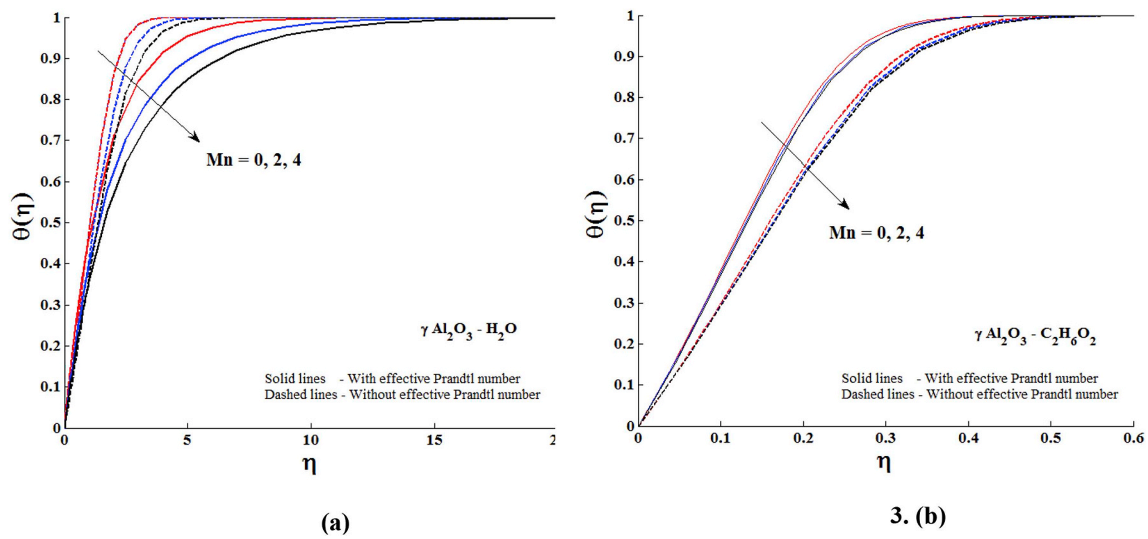

Fig. 3. Effect of magneitc paramete (Mn) on temperature with $\phi = 0.1$, Rd = 2.5, $\theta_w = 1.5$ and M = 2 (a) γ $Al_2O_3 - H_2O$ with $Pr = 6.96$ (b) γ $Al_2O_3 - C_2H_6O_2$ with $Pr = 204$.

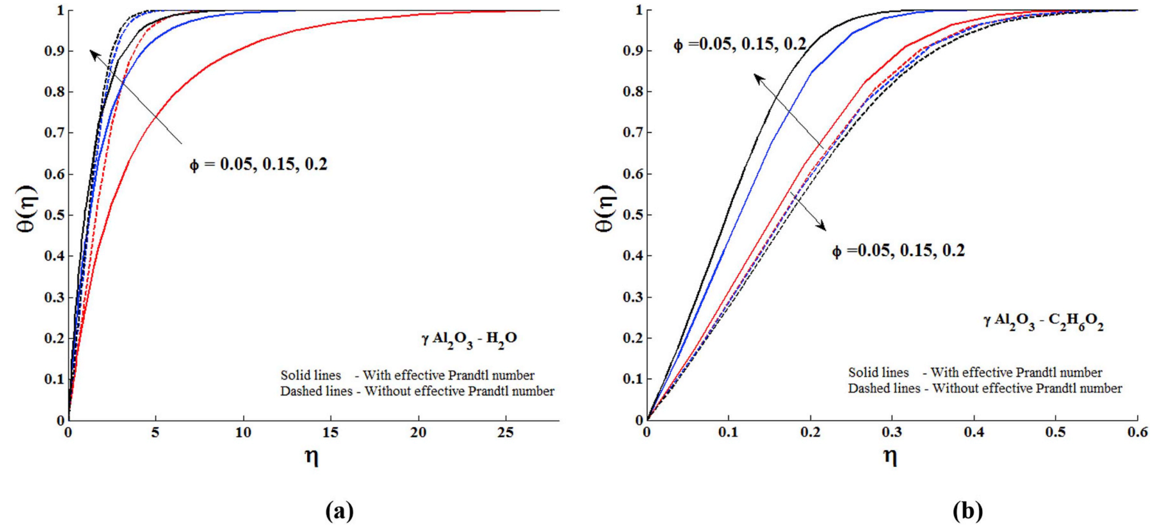

Fig. 4. Effect of nanoparticle volume fraction parameter (ϕ) on temperature with Mn = 4, Rd = 2.5, θ_w = 1.5 and M = 2 (a) γ Al_2O_3 − H_2O with *Pr* = 6.96 (b) γ Al_2O_3 − $C_2H_6O_2$ with *Pr* = 204.

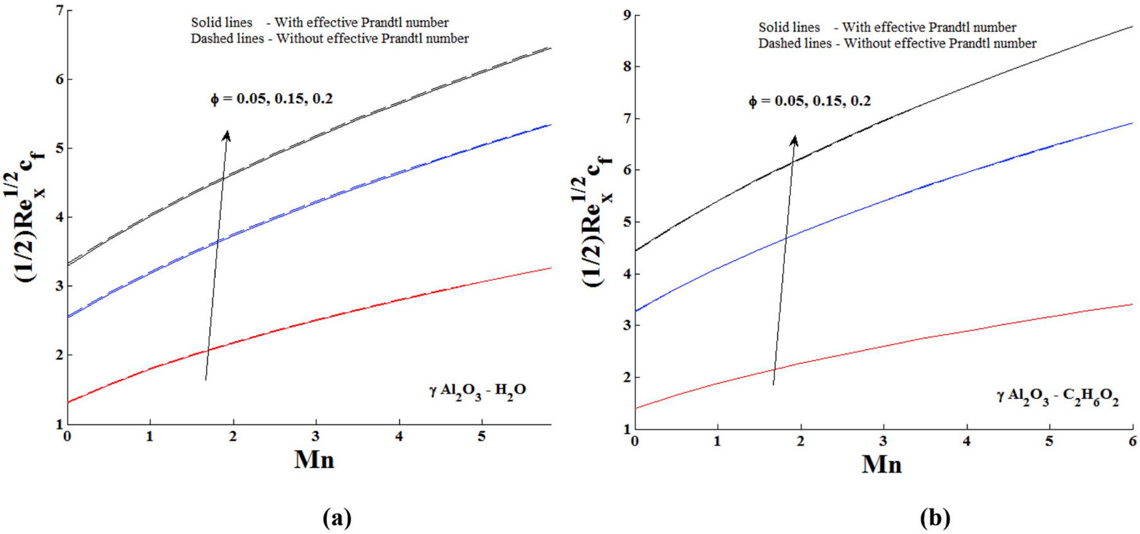

Fig. 5. Effect of magnetic parameter (Mn) and nanoparticle volume fraction (ϕ) on local skin friction coefficient with θ_w = 1.5, Rd = 2.5 and M = 2 (a) γ Al_2O_3 − H_2O with *Pr* = 6.96 (b) γ Al_2O_3 − $C_2H_6O_2$ with *Pr* = 204.

5. Conclusion

In the present research, the influences of an effective Prandtl number on the melting heat transfer of Water/Ethylene glycol based γ Al_2O_3 nanofluids over a stretching sheet with magnetic field effects are investigated. Melting heat transfer boundary condition is derived in the presence of effective *Pr*. Numerical solutions are obtained for the governing ODE's using the IPS method with shooting technique. The significant results noticed from the present study are as follows:

- The consideration of effective *Pr* leads to increase the thickness of Nano-momentum boundary layer.
- The presence of effective *Pr* increases the nanothermal boundary layer thickness of γ Al_2O_3 - *Ethylene glycol* nanofluid and decreases the nanoboundary layer thickness of γ Al_2O_3-*Water* nanofluid.
- The nanothermal boundary layer thickness of γ Al_2O_3-*Water* decreases in the absence of effective *Pr* and the nanothermal boundary layer thickness of γ Al_2O_3 - *Ethylene glycol* increases in the absence of effective *Pr*.
- The increments in melting parameter decrease the temperature profile and increase the thickness of the nanothermal boundary layers of γ Al_2O_3-Water and γ Al_2O_3- *Ethylene glycol* nanofluids.
- The magnitude of skin friction coefficient increases for γ Al_2O_3- *Ethylene glycol* and decreases for γ Al_2O_3-*Water* in the presence of

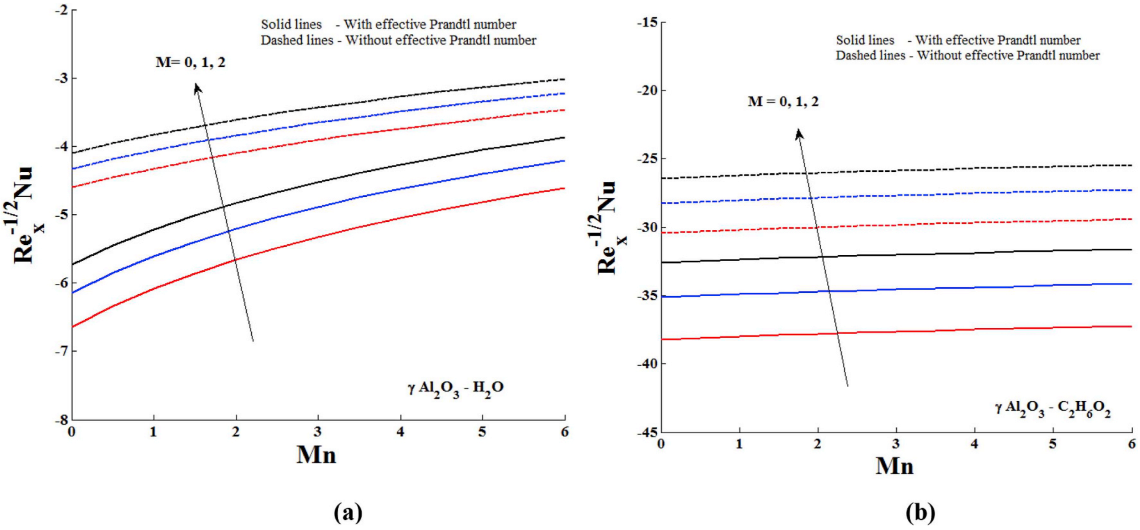

Fig. 6. Effect of magnetic parameter (Mn) and melting parameter (M) on reduced Nusselt number with $\phi = 0.1$, $\theta_w = 1.5$ and Rd = 2.5 (a) γ Al_2O_3 − H_2O with $Pr = 6.96$ (b) γ Al_2O_3 − $C_2H_6O_2$ with $Pr = 204$.

effective *Pr*.

➢ The magnitude of reduced Nusselt number increases with magnetic parameter and melting parameter and decreases with nanoparticle volume fraction parameter and radiation parameter for both γ Al_2O_3-*Water* and γ Al_2O_3- *Ethylene glycol* nanofluids.
➢ Both nanomomentum and nanothermal boundary layers can be controlled by effective *Pr*.

Acknowledgment

The authors wish to express their sincere thanks to the honourable referees for their valuable comments and suggestions to improve the quality of the paper. In addition Authors would like to acknowledge and express their gratitude to the United Arab Emirates University, Al Ain, UAE for providing the financial support with Grant No. 31S240-UPAR (2) 2016.

References

[1] S.U.S. Choi, Enhancing thermal conductivity of fluids with nanoparticles, developments and applications of non-Newtonian flows, Fed. Times 231 (1995) 99–105 MDvol. 66.
[2] M.A.A. Hamad, Analytical solution of natural convection flow of a nanofluid over a linearly stretching sheet in the presence of magnetic field, Int. Commun. Heat. Mass. 38 (2011) 487–492.
[3] M. Turkyilmazoglu, Exact analytical solutions for heat and mass transfer of MHD slip flow in nanofluids, Chem. Eng. Sci. 84 (2012) 182–187.
[4] P.K. Kameswaran, M. Narayana, P. Sibanda, P.V.S.N. Murthy, Hydromagnetic nanofluid flow due to a stretching or shrinking sheet with viscous dissipation and chemical reaction effects, Int. J. Heat Mass Transf. 55 (2012) 7587–7595.
[5] K. Vajravelu, K.V. Prasad, Jinho Lee, Changhoon Lee, I. Pop, A. Robert Van Gorder, Convective heat transfer in the flow of viscous Ag-water and Cu- water nanofluids over a stretching surface, Int. J. Therm. Sci. 50 (2011) 843–851.
[6] A.K.A. Hakeem, N. Vishnu Ganesh, B. Ganga, Magnetic field effect on second order slip flow of nanofluid over a stretching/shrinking sheet with thermal radiation effect, J. Magn. Magn Mater. 381 (2015) 243–257.
[7] S.N. Reddy, A. Chamkha, Influence of size, shape, type of nanoparticles, type and temperature of the base fluid on natural convection MHD of nanofluids, Alexandria Eng. J. 55 (1) (2016) 331–341.
[8] S.N. Reddy, A. Chamkha, Soret and Dufour effects on MHD convective flow of Al_2O_3–water and TiO_2–water nanofluids past a stretching sheet in porous media with heat generation/absorption, Adv. Powder Technol. 27 (4) (2016) 1207–1218.
[9] F. Shahzad, R. Ul Haq, Q. Al-Mdallal, Water driven Cu nanoparticles between two concentric ducts with oscillatory pressure gradient, J. Mol. Liq. 224 (2016) 332.
[10] N. Sandeep, C. Sulochana, B. Rushi Kumar, Unsteady MHD radiative flow and heat transfer of a dusty nanofluid over an exponentially stretching surface, Eng. Sci. Technol. Int J. 19 (1) (2016) 227–240.
[11] M. Sheikholeslami, M.M. Rashidi, D. M.Al Saad, F. Firouzi, H.B. Rokni, Steady nanofluid flow between parallel plates considering thermophoresis and brownian effects, J. King Saud Univ. Sci. 28 (2016) 380–389.
[12] I. Rashid, R. Ul Haq, Z.H. Khan, Q. Al-Mdallal, Flow of water based alumina and copper nanoparticles along a moving surface with variable temperature, J. Mol. Liq. 246 (2017) 354–362.
[13] I. Rashid, R. Ul Haq, Q. Al-Mdallal, Aligned magnetic field effects on water based metallic nanoparticles over a stretching sheet with PST and thermal radiation effects, Phys. E Low Dimen. Syst. Nanostruct. 89 (2017) 33–42.
[14] S. Aman, I. Khan, Z. Ismail, M.Z. Salleh, Q. Al-Mdallal, Heat transfer enhancement in free convection flow of CNTs Maxwell nanofluids with four different types of molecular liquids, Sci. Rep. 7 (2017) Article number: 2445.
[15] S.R. Mishra, I. Khan, Q. Al-Mdallal, Q. Asifa, Free convective micropolar fluid flow and heat transfer over a shrinking sheet with heat source, Case Stud. Therm. Eng. 11 (2018) 113–119.
[16] M. Qasim, Z.H. Khan, I. Khan, Q. Al-Mdallal, Analysis of entropy generation in flow of methanol-based nanofluid in a sinusoidal wavy channel, Entropy 19 (10) (2017) 490.
[17] R. Haq, Z. Hammouch, W.A. Khan, Water-based squeezing flow in the presence of carbon nanotubes between two parallel disks, Therm. Sci. 20 (6) (2016) 1973–1981.

[18] Z.H. Khan, S.T. Hussain, Z. Hammouch, Flow and heat transfer analysis of water and ethylene glycol based Cu nanoparticles between two parallel disks with suction/injection effects, J. Mol. Liq. 221 (2016) 298–304.
[19] A. Shafiq, Z. Hammouch, T.N. Sindhu, Bioconvective MHD flow of tangent hyperbolic nanofluid with Newtonian heating, Int. J. Mech. Sci. 133 (2017) 759–766.
[20] F.A. Soomro, Z. Hammouch, Heat transfer analysis of CuO-water enclosed in a partially heated rhombus with heated square obstacle, Int. J. Heat Mass Transf. 118 (2018) 773–784.
[21] R. Haq, F.A. Soomro, Z. Hammouch, Heat exchange within the partially heated C-shape cavity filled with the water based SWCNTs, Int. J. Heat Mass Transf. 127 (2018) 506–514.
[22] F. Mabood, A. Mastroberardino, Melting heat transfer on MHD convective flow of a nanofluid over a stretching sheet with viscous dissipation and second order slip, J. Taiwan. Inst. Chem. Eng. 57 (2015) 62–68.
[23] T. Hayat, Z. Hussain, A. Alsaedi, B. Ahmad, Heterogeneous- homogeneous reactions and melting heat transfer effects in flow with carbon nanotubes, J. Mol. Liq. 220 (2016) 200–207.
[24] B.J. Gireesha, B. Mahanthesh, I.S. Shivakumara, K.M. Eshwarappa, Melting heat transfer in boundary layer stagnation-point flow of nanofluid toward a stretching sheet with induced magnetic field, Eng. Sci. Technol. Int J. 19 (2016) 313–321.
[25] T. Chakraborty, K. Das, P. Kundu, Analytical approach to a Jeffrey nanofluid flow towards a Stagnation point coexisting with Magnetic field and Melting heat effects, J. Mol. Liq. 229 (2017) 443–452.
[26] S. Aman, Q. Al-Mdallal, I. Khan, Heat transfer and second order slip effect on MHD flow of fractional Maxwell fluid in a porous medium, J. King Saud Univ. Sci. (2016), https://doi.org/10.1016/j.jksus.2018.07.007.
[27] Q. Al-Mdallal, K.A. Abro, I. Khan, Analytical Solutions of Fractional Walter's B Fluid with Applications, Complexity, 2018 Article ID 8131329.
[28] S.E.B. Maiga, S.E.B. Palm, C.T. Nguyen, G. Roy, N. Galanis, Heat transfer enhancement by using nanofluids in forced convection flows, Int. J. Heat Fluid Flow 26 (2005) 530–546.
[29] S.E.B. Maiga, C.T. Nguyen, N. Galanis, G. Roy, Heat transfer behaviours of nanofluids in a uniformly heated tube, Superlattice. Microst. 35 (2004) 543–557.
[30] S.E.B. Maiga, C.T. Nguyen, N. Galanis, G. Roy, Heat transfer enhancement in forced convection laminar tube flow by using nanofluids, Proc. CHT-04 ICHMT Int. Symposium Advances Computational Heat Transfer, April 19-24 Norway, 2004 Paper No. CHT-04-101, 25pp..
[31] I. Pop, C.V., S. Fohanno, G. Polidori, C.T. Nguyen, Analysis of laminar-to- turbulent threshold with water γ Al_2O_3 and ethylene glycol- γ Al_2O_3 nanofluids in free convection, Proceedings of the 5th IASME/WSEAS Int. Conference on Heat Transfer, Thermal Engineering and Environment, Athens, Greece, August 25–27, 2007, 2007, p. 188.
[32] B. Farajollahi, S.Gh Etemad, M. Hojjat, Heat transfer of nanofluids in a shell and tube heat exchanger, Int. J. Heat Mass Transf. 53 (2010) 12–17.
[33] T.M.O. Sow, S. Halelfadl, S. Lebourlout, C.T. Nguyen, Experimental study of the freezing point of γ- Al_2O_3 water nanofluid, Adv. Mech. Eng. (2012) Article ID 162961.
[34] H. Beiki, M.N. Esfahany, N. Etesami, Laminar forced convective mass transfer of γ-Al_2O_3/electrolyte nanofluid in a circular tube, Int. J. Therm. Sci. 64 (2013) 251–256.
[35] E. Esmaeilzadeh, H. Almohammadi, A. Nokhosteen, A. Motezaker, A.N. Omrani, Study on heat transfer and friction factor characteristics of γ-Al_2O_3/water through circular tube with twisted tape inserts with different thicknesses, Int. J. Therm. Sci. 82 (2014) 72–83.
[36] M. Abdul-Aziz, H.A. Azza, H. Elkhatib, S.H. Othman, Effect of operating parameters on the transient behaviour of gravity-assisted heat-pipe using radio chemically prepared γ Al_2O_3 nano-fluid, Adv. Powder Technol. 27 (2016) 1651–1662.
[37] A.M. Bayomy, M.Z. Saghir, Experimental study of using γ-Al_2O_3–water nanofluid flow through aluminum foam heat sink: comparison with numerical approach, Int. J. Heat Mass Transf. 107 (2017) 181–203.
[38] H.S. Moghaieb, H.M. Abdel-Hamid, M.H. Shedid, A.B. Helali, Engine cooling using γAl2O3/water nanofluids, Appl. Therm. Eng. 115 (2017) 152–159.
[39] N. Vishnu Ganesh, A.K. Abdul Hakeem, B. Ganga, A comparative theoretical study on Al_2O_3 and γ-Al_2O_3 nanoparticles with different base fluids over a stretching sheet, Adv. Powder Technol. 27 (2) (2016) 436–441.
[40] M.M. Rashidi, N. Vishnu Ganesh, A.K. Abdul Hakeem, B. Ganga, G. Lorenzini, Influences of an effective Prandtl number model on nano boundary layer flow of γ Al_2O_3–H_2O and γ Al_2O_3–$C_2H_6O_2$ over a vertical stretching sheet, Int. J. Heat Mass Transf. 98 (2016) 616–623.
[41] N. Vishnu Ganesh, P.K. Kameswaran, Q. Al-Mdallal, A.K. Hakeem, B. Ganga, Non-linear thermal radiative Marangoni boundary layer flow of gamma Al_2O_3 nanofluids past a stretching sheet, J. Nanofluids 7 (5) (2018) 944–950.
[42] N. Vishnu Ganesh, A. Chamkha, Q. Al-Mdallal, P.K. Kameswaran, Magneto - Marangoni nano-boundary layer flow of water and ethylene glycol based γ *Al2O3* nanofluids with non-linear thermal radiation effects, Case Stud. Therm. Eng. 12 (2018) 340–348.
[43] R. Cortell, Fluid flow and radiative nonlinear heat transfer over a stretching sheet, J. King Saud Univ. Sci. 26 (2) (2014) 161–167.
[44] N. Vishnu Ganesh, Qasem M. Al-Mdallal, Ali J. Chamkha, A numerical investigation of Newtonian fluid flow with buoyancy, thermal slip of order two and entropy generation, Case Stud. Therm. Eng. 13 (2019) Article 100376.
[45] U. Al Khawaja, Q. Al-Mdallal, Convergent power Series of and solutions to nonlinear differential equations, Int. J. Diff. Equ. (2018) 2018. Article ID 6043936.
[46] L.Y. Al Sakkaf, Q. Al-Mdallal, U. Al Khawaja, A Numerical Algorithm for Solving Higher-Order Nonlinear BVPs with an Application on Fluid Flow over a Shrinking Permeable Infinite Long Cylinder, Complexity, 2018 Article ID 8269541.